Emulation of a Quantum Spin with a Superconducting Phase Qudit

Matthew Neeley *et al.*

Science **325**, 722 (2009);
DOI: 10.1126/science.1173440

CORRECTED 23 OCTOBER 2009; SEE LAST PAGE

10. A. Decourchelle, D. C. Ellison, J. Ballet, *Astrophys. J.* **543**, L57 (2000).
11. J. Vink, in *High Energy Gamma-Ray Astronomy: Proceedings of the 4th International Meeting on High Energy Gamma-Ray Astronomy* (American Institute of Physics, College Park, MD, 2008), vol. 1085, pp. 169–180.
12. L. O'C. Drury, F. A. Aharonian, D. Malyshev, S. Gabici, *Astron. Astrophys.* **496**, 1 (2009).
13. D. J. Patnaude, D. C. Ellison, P. Slane, *Astrophys. J.* **696**, 1956 (2009).
14. J. P. Hughes, C. E. Rakowski, A. Decourchelle, *Astrophys. J.* **543**, L61 (2000).
15. G315.4-2.3, MSH 14-*63*.
16. F. Aharonian *et al*., *Astrophys. J.* **692**, 1500 (2009).
17. F. R. Stephenson, D. A. Green, *Historical Supernovae and Their Remnants*, International Series in Astronomy and Astrophysics, vol. 5 (Oxford Univ. Press, Oxford, 2002).
18. J. Vink *et al*., *Astrophys. J.* **648**, L33 (2006).
19. J. Vink, J. S. Kaastra, J. A. M. Bleeker, *Astron. Astrophys.* **328**, 628 (1997).
20. R. A. Chevalier, R. P. Kirshner, J. C. Raymond, *Astrophys. J.* **235**, 186 (1980).
21. L. O'C Drury, P. Duffy, J. G. Kirk. *Astron. Astrophys.* **309**, 1002 (1996).
22. P. F. Winkler, G. Gupta, K. S. Long, *Astrophys. J.* **585**, 324 (2003).
23. I. Appenzeller *et al*., *Messenger* **94**, 1 (1998).
24. M. Rosado, P. Ambrocio-Cruz, E. Le Coarer, M. Marcelin, *Astron. Astrophys.* **315**, 243 (1996).
25. J. Sollerman, P. Ghavamian, P. Lundqvist, R. C. Smith, *Astron. Astrophys.* **407**, 249 (2003).
26. V. V. Dwarkadas, *Astrophys. J.* **630**, 892 (2005).
27. The effects of cosmic ray acceleration on the evolution of the forward shock are small; see (*13*).
28. K. S. Long, W. P. Blair, *Astrophys. J.* **358**, L13 (1990).
29. P. Ghavamian, J. Raymond, R. C. Smith, P. Hartigan, *Astrophys. J.* **547**, 995 (2001).
30. F. A. Aharonian, A. M. Atoyan, *Astron. Astrophys.* **351**, 330 (1999).
31. S. Katsuda, H. Tsunemi, K. Mori, *Astrophys. J.* **678**, L35 (2008).
32. B. E. Westerlund, *Astrophys. J.* **74**, 879 (1969).
33. J. Brand, L. Blitz, *Astron. Astrophys.* **275**, 67 (1993).
34. K. Matsunaga *et al*., *Publ. Astron. Soc. Jpn.* **53**, 1003 (2001).
35. K. Heng, R. McCray, *Astrophys. J.* **654**, 923 (2007).
36. M. van Adelsberg, K. Heng, R. McCray, J. C. Raymond, *Astrophys. J.* **689**, 1089 (2008).
37. P. Ghavamian, J. M. Laming, C. E. Rakowski, *Astrophys. J.* **654**, L69 (2007).
38. J. C. Raymond, P. A. Isenberg, J. M. Laming, *Astrophys. J.* **682**, 408 (2008).
39. P. Ghavamian, J. Raymond, P. Hartigan, W. P. Blair, *Astrophys. J.* **535**, 266 (2000).
40. J.-J. Lee *et al*., *Astrophys. J.* **659**, L133 (2007).
41. A. Y. Wagner, J.-J. Lee, J. C. Raymond, T. W. Hartquist, S. A. E. G. Falle, *Astrophys. J.* **690**, 1412 (2009).
42. R. C. Smith, R. P. Kirshner, W. P. Blair, P. F. Winkler, *Astrophys. J.* **375**, 652 (1991).
43. R. A. Chevalier, *Astrophys. J.* **272**, 765 (1983).
44. A. M. Bykov, K. Dolag, F. Durret, *Space Sci. Rev.* **134**, 119 (2008).
45. M. A. Malkov, L. Drury, *Rep. Prog. Phys.* **64**, 429 (2001).
46. M. A. Malkov, *Astrophys. J.* **511**, L53 (1999).
47. J.-L. Starck, F. Murtagh, A. Bijaoui, *Image Processing and Data Analysis. The Multiscale Approach* (Cambridge Univ. Press, Cambridge, 1998).

48. We thank A. Achterberg for a useful discussion of the current literature on the theory of shock heating. E.A.H. and J.V. are supported by the Vidi grant to J.V. from the Netherlands Organization for Scientific Research (NWO). This work was supported in part by Grant-in-Aid for Scientific Research from the Japanese Ministry of Education, Culture, Sports, Science and Technology, no. 194014 (A.B.) and no. 19047004 and 21740184 (R.Y.). S.F. is supported by Smithsonian Astrophysical Observatory grant G07-8073X. P.G. is supported by the Space Telescope Science Institute grant GO-11184.07. This paper is based in part on observations made with European Southern Observatory Telescopes at the Paranal Observatories under program ID 079.D-0735.

Supporting Online Material

www.sciencemag.org/cgi/content/full/1173383/DC1
SOM Text
Fig. S1
Tables S1 and S2
References

11 March 2009; accepted 15 June 2009
Published online 25 June 2009;
10.1126/science.1173383
Include this information when citing this paper.

Emulation of a Quantum Spin with a Superconducting Phase Qudit

Matthew Neeley,[1] Markus Ansmann,[1] Radoslaw C. Bialczak,[1] Max Hofheinz,[1] Erik Lucero,[1] Aaron D. O'Connell,[1] Daniel Sank,[1] Haohua Wang,[1] James Wenner,[1] Andrew N. Cleland,[1] Michael R. Geller,[2] John M. Martinis[1]*

In quantum information processing, qudits (*d*-level systems) are an extension of qubits that could speed up certain computing tasks. We demonstrate the operation of a superconducting phase qudit with a number of levels *d* up to *d* = 5 and show how to manipulate and measure the qudit state, including simultaneous control of multiple transitions. We used the qudit to emulate the dynamics of single spins with principal quantum number *s* = 1/2, 1, and 3/2, allowing a measurement of Berry's phase and the even parity of integer spins (and odd parity of half-integer spins) under 2π-rotation. This extension of the two-level qubit to a multilevel qudit holds promise for more-complex quantum computational architectures and for richer simulations of quantum mechanical systems.

Quantum computers are typically thought of as being composed of qubits, or two-level quantum systems (*1*). However, one can also use qutrits (three-level systems) or more generally qudits (*d*-level systems), which can simplify some quantum computations (*2*, *3*) and improve quantum cryptography (*4*). The advantages of qudits are also evident when one considers using a quantum computer not to perform computations but rather to emulate another quantum system by the direct implementation of an analogous physical Hamiltonian. This requires a map between the Hilbert space and unitary operators of the emulator and the target system. If the target system contains parts with $d > 2$ levels, then it maps much more naturally to a set of qudits, making a qudit emulator potentially more efficient.

We describe the operation of a superconducting phase qudit with full unitary control and measurement of the state (*5*, *6*). This device, one of a family of superconducting quantum information–processing devices (*7*), is typically operated as a qubit (*8*, *9*) by restricting it to the two lowest-energy eigenstates. By relaxing this restriction, we can operate it as a qudit in which the number of levels *d* can be chosen as desired, in this case up to $d = 5$.

Emulation of spin, or intrinsic angular momentum, naturally calls for qudits with $d > 2$. A spin state is described by two quantum numbers (*10*), the principal quantum number $s = 0, 1/2, 1, 3/2,...$ and the azimuthal quantum number *m*, limited to the $d = 2s + 1$ values $m = s, s - 1,..., -s$. For a given *s*, the general spin states $|\psi\rangle = \sum_m c_m|s,m\rangle$ span a *d*-dimensional Hilbert space, so that although qubits can be used to model spin-1/2 physics a qudit allows one to model spins $s \geq 1$ ($d \geq 3$).

When rotated about a closed path (Fig. 1), a spin state $|s,m\rangle$ acquires a phase factor $\exp(-im\Omega)$, where Ω is the solid angle enclosed by the path, as predicted by Berry (*11*–*13*). For a 2π-rotation ($\Omega = 2\pi$), integer spins are unchanged, whereas half-integer spins are multiplied by −1. This parity difference leads to the symmetric statistics of bosons (or antisymmetric statistics of fermions) under exchange, as described by the spin-statistics theorem (*14*, *15*). The effect of 2π-rotations was first observed on spins $s = 1/2$ via neutron interferometry (*16*, *17*) and later for $s = 1$ and $s = 3/2$ in nuclear magnetic resonance (*18*). In superconducting qubits, the spin-1/2 parity (*19*) and Berry's phase (*20*) have been measured. We measured Berry's phase and spin parity for spin-1/2, spin-1, and spin-3/2 at all solid angles using our qudit emulation (*21*).

Our flux-biased phase qudit (Fig. 2A) is a nonlinear resonator formed by a Josephson junction, inductor, and capacitor. Applied magnetic flux produces a cubic potential as a function of the junction phase δ, with barrier height ΔU that can be tuned so as to change the number of energy levels in the well (Fig. 2B). The cubic anharmonicity is crucial for qubit operation (*22*), allowing microwaves at frequency $\omega_{10} = (E_1 - E_0)/\hbar$ to drive transitions between $|0\rangle$ and $|1\rangle$ while minimizing "leakage" to $|2\rangle$ and higher (*23*). For measurement, a brief current pulse $I_{\mathrm{meas}}^{(1)}$ is ap-

[1]Department of Physics, University of California at Santa Barbara (UCSB), Santa Barbara, CA 93106, USA. [2]Department of Physics and Astronomy, University of Georgia, Athens, GA 30602, USA.

*To whom correspondence should be addressed. E-mail: martinis@physics.ucsb.edu

plied to lower the barrier and cause $|1\rangle$ (but not $|0\rangle$) to tunnel out of the well. An on-chip superconducting quantum interference device (SQUID) detects this tunneling (*24*).

For qudit operation, anharmonicity is again crucial because it ensures that all transition frequencies $\omega_{n,n-1} = (E_n - E_{n-1})/\hbar$ are distinct, allowing frequency-selective control of all qudit states. In the present sample, transition frequencies are ~6 GHz and separated from each other by ~200 MHz (Fig. 2B). This separation is large enough that transitions can be selectively driven with fast pulses (as compared with the state lifetimes) but small enough that the total bandwidth required is within that of our microwave control (*13*). This selective control of transitions between neighboring levels allows for the construction of arbitrary unitary gates on the d-level qudit manifold (*25*).

To measure the qudit, $d-1$ pulse amplitudes $I^{(1)}_{\mathrm{meas}} > I^{(2)}_{\mathrm{meas}} > \ldots > I^{(d-1)}_{\mathrm{meas}}$ are chosen (Fig. 2C), with each pulse $I^{(n)}_{\mathrm{meas}}$ adjusted so that the upper states $|n\rangle$, $|n+1\rangle$,... tunnel out of the well whereas the lower states $|n-1\rangle$, $|n-2\rangle$,... do not. Each tunneling measurement is repeated ~10^3 times on identically prepared qudit states in order to obtain the cumulative tunneling probability $P_{\geq n}$. From these, we obtain the individual occupation probabilities $P_n = P_{\geq n} - P_{\geq n+1}$, which are the diagonal elements $P_n = \rho_{nn}$ of the qudit density matrix $\rho_{mn} = \langle m|\hat{\rho}|n\rangle$.

Arbitrary unitary gates combined with state measurement make this system a universal single qudit (*5*, *25*). By applying an appropriate set of unitaries before measurement, one could for example reconstruct the entire qudit density matrix, similar to previously demonstrated single- and coupled-qubit state tomography (*8*, *9*). Qudit-qudit coupling (*25*) is also possible but beyond the scope of this work.

We calibrated the qudit one transition at a time from the ground state upwards. First, as for qubit operation, we initialized the system in $|0\rangle$, and a standard protocol (*23*) was used to find $I^{(1)}_{\mathrm{meas}}$ and ω_{10} and to calibrate a π-pulse $|0\rangle \rightarrow |1\rangle$. Next, we applied this π-pulse so as to initialize the system in $|1\rangle$ and repeated the protocol so as to find $I^{(2)}_{\mathrm{meas}}$ and ω_{21} and to calibrate a π-pulse $|1\rangle \rightarrow |2\rangle$. This process may be repeated as desired, in this case up to $|d-1\rangle = |4\rangle$. Each π-pulse has a 16-ns envelope (*13*), with the amplitudes scaled to equalize the rotation rates (Fig. 3, A to C), thus calibrating the transition matrix elements $\delta_{n,n-1} = \langle n|\hat{\delta}|n-1\rangle$. The measured lifetimes of the excited states are $T_1 = 610$ ns, $T_2 = 320$ ns, $T_3 = 220$ ns, and $T_4 = 170$ ns, which is in good agreement with the $T_n = T_1/n$ scaling seen in harmonic oscillators (*26*, *27*) because of the weak anharmonicity.

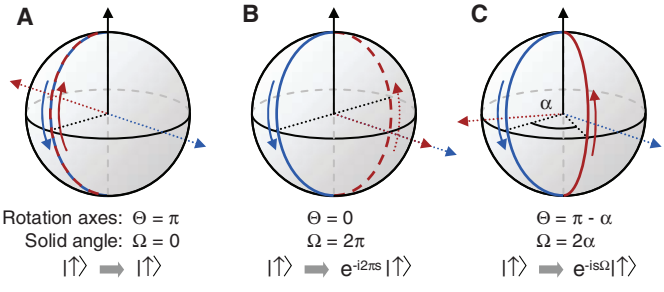

Fig. 1. Effect of rotation on a spin. The spin begins in the up state $|\uparrow\rangle = |s,+s\rangle$. After two π-rotations (blue and red) with angle Θ between the rotation axes (dotted arrows), the spin returns to $|\uparrow\rangle$ with a phase factor depending on Θ and s. In (**A**), the second rotation reverses the first, giving a phase factor 1, which leaves the spin state unchanged. In (**B**), both rotations are about the same axis. The spin traces out a great circle and acquires a phase factor $\exp(-i2\pi s)$. For integer spins (bosons), this has no effect, but for half-integer spins (fermions) this gives a factor of -1. In the general case (**C**), the acquired phase factor is $\exp(-is\Omega)$, where $\Omega = 2\alpha$ is the enclosed solid angle.

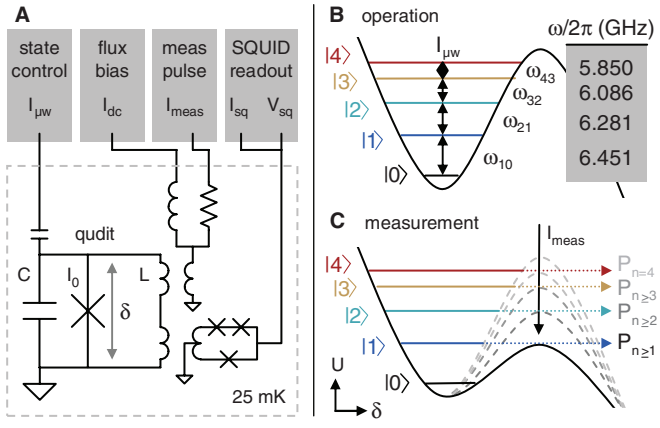

Fig. 2. Operation and measurement of a superconducting phase qudit. (**A**) Schematic of qudit circuit and control electronics. Current I_{dc} biases the junction, microwave drive $I_{\mu\mathrm{w}}$ manipulates the qudit state, and an on-chip SQUID detects tunneling events for readout. (**B**) The potential energy as a function of junction phase δ forms a well with several energy levels. The frequencies $\omega_{n,n-1} = (E_n - E_{n-1})/\hbar$ are distinct, allowing transitions to be driven independently. (**C**) For measurement, a brief current pulse $I^{(1)}_{\mathrm{meas}}$ is applied so as to lower the potential energy barrier, causing states $|n\rangle$, $|n+1\rangle$,... to tunnel out of the well. For each n, this is repeated ~10^3 times in order to obtain a probability.

Evolution of the qudit state is best described in the basis of moving eigenkets $|n'\rangle = \exp(-iE_n t/\hbar)|n\rangle$. In this basis, microwaves at $\omega_{n,n-1}$ appear as off-diagonal elements in the Hamiltonian

$$H' = \begin{pmatrix} 0 & A^*_{10} & 0 & 0 \\ A_{10} & 0 & A^*_{21} & 0 \\ 0 & A_{21} & 0 & A^*_{32} \\ 0 & 0 & A_{32} & 0 \end{pmatrix} \quad (1)$$

where the $A_{n,n-1}$ are arbitrary complex numbers giving the amplitude and phase of the microwaves at $\omega_{n,n-1}$, and we have made the usual rotating-wave approximation by discarding off-resonant terms. The calibration shown in Fig. 3, A to C, ensures that the $A_{n,n-1}$ are calibrated relative to each other.

To emulate a spin rotation, the applied qudit Hamiltonian should be the appropriate rotation generator. The generators of rotation about X for $s = 1/2$, 1, and 3/2 (*10*) are

$$X^{(1/2)} = \begin{pmatrix} 0 & 1 \\ 1 & 0 \end{pmatrix}$$

$$X^{(1)} = \begin{pmatrix} 0 & 1 & 0 \\ 1 & 0 & 1 \\ 0 & 1 & 0 \end{pmatrix}$$

$$X^{(3/2)} = \begin{pmatrix} 0 & \frac{\sqrt{3}}{2} & 0 & 0 \\ \frac{\sqrt{3}}{2} & 0 & 1 & 0 \\ 0 & 1 & 0 & \frac{\sqrt{3}}{2} \\ 0 & 0 & \frac{\sqrt{3}}{2} & 0 \end{pmatrix} \quad (2)$$

where the largest element in each matrix has been normalized to 1. Generators of Y-rotation are similar but have imaginary off-diagonal terms. These operators all have the form Eq. 1 of microwave-drive Hamiltonians, allowing us to use microwaves to emulate spin rotations about X, Y, or any other axis in the X-Y plane.

The evolution of the qudit state under emulated spin rotation is shown in Fig. 3 for spin-1 (Fig. 3D) and spin-3/2 (Fig. 3E). In both cases, the ground state $|0\rangle$ is reserved as a phase reference, so the spin is mapped to $|1\rangle \equiv |s,s\rangle$, $|2\rangle \equiv |s,s-1\rangle$,..., $|1+2s\rangle \equiv |s,-s\rangle$. The spin starts in $|1\rangle$, rotates to $|3\rangle$ (spin-1) or $|4\rangle$ (spin-3/2), then back to $|1\rangle$ and so on. Although the state populations evolve in a complicated fashion, the expectation value $\langle \hat{Z} \rangle = \sum_m m\, P_{|s,m\rangle}$ evolves sinusoidally (dashed line), as is expected for a rotating spin. Compared with spin-1/2 (Fig. 3, A to C), the rotation is slowed by a factor of $\sqrt{2}$ (spin-1) or 2 (spin-3/2), which is in agreement with direct exponentiation of the matrices in Eq. 2.

Next, these emulated spin rotations are used to measure Berry's phase, as described in Fig. 1. We made the phase measurement using Ramsey interference with $|0\rangle$ as a reference. First, we applied a $\pi/2$-pulse in order to prepare the superposition $(|0\rangle + |1\rangle)/\sqrt{2}$. Then,

we applied two emulated π-pulses with angle Θ between their rotation axes, rotating the spin component $|1\rangle \equiv |s,s\rangle$ about a closed path and giving the state $[|0\rangle + \exp(-is\Omega)|1\rangle]/\sqrt{2}$. Finally, we applied a second π/2-pulse in order to detect the phase of $|1\rangle$. Because the rotation axis ϕ of the latter π/2-pulse is varied, P_1 traces out a sinusoid—a Ramsey fringe—whose phase corresponds to the acquired spin phase.

The result of this experiment is shown in Fig. 4. For spin-0, no π-rotations are performed (the rotation generator is $X^{(0)} = 0$), so the Ramsey fringes are stationary. For s = 1/2, 1, and 3/2, the Ramsey fringes shift by −2π, −4π, and −6π, respectively, as Θ increases from 0 to 2π (Ω changes by 4π), which is in agreement with the predicted Berry phase factor $\exp(-is\Omega)$. The slices at Θ = π (Ω = 0) and Θ = 0 (Ω = 2π) clearly show the parity difference between integer spins s = 0, 1, and half-integer spins s = 1/2, 3/2, with in- and out-of-phase Ramsey fringes, respectively.

The Ramsey fringes show reduced contrast when higher qudit states are used in the sequence, which is largely due to the reduced lifetimes $T_n \approx T_1/n$ of the higher states. In addition, the use of higher states leads to imperfections in the microwave control because of the large bandwidth required and the effect of off-resonant terms dropped from Eq. 1. Ongoing work to reduce decoherence in superconducting quantum circuits (*28*) will improve the state lifetimes, and the off-resonant terms could be taken into account so as to improve the fidelity of qudit operation (*22*).

We have shown that the superconducting phase qubit can be extended to operate as a qudit up to d = 5 levels. The qudit state can be readily manipulated and measured with our existing control electronics, allowing us to perform nontrivial qudit protocols in order to emulate spins s = 1/2, 1, and 3/2. We reproduced the quantum

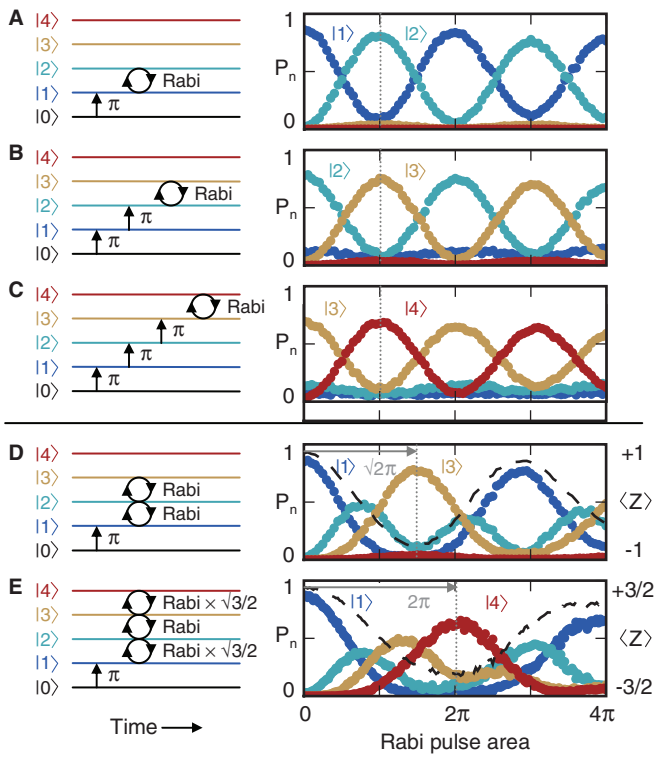

Fig. 3. Manipulation of the qudit state with microwaves. **(A)** (Left) The pulse sequence used to calibrate microwaves $|1\rangle \rightarrow |2\rangle$. A π-pulse excites the qubit to $|1\rangle$, then a second pulse drives Rabi oscillations between $|1\rangle$ and $|2\rangle$. (Right) Occupation probabilities P_n plotted versus the integrated area of the Rabi pulse, where π corresponds to a standard 16-ns pulse envelope with amplitude adjusted so as to create a π-rotation (swap) from $|1\rangle$ to $|2\rangle$. **(B** and **C)** Similar calibration for $|2\rangle \rightarrow |3\rangle$ and $|3\rangle \rightarrow |4\rangle$. **(D)** (Left) The pulse sequence for generating spin-1 rotations by simultaneously driving $|1\rangle \rightarrow |2\rangle$ and $|2\rangle \rightarrow |3\rangle$. (Right) A plot of P_n versus the integrated pulse area of the single drives. The spin-1 π-rotation (from $|1\rangle$ to $|3\rangle$) is $\sqrt{2}$ longer than a spin-1/2 rotation. The dashed line shows $\langle \hat{Z} \rangle$, which varies sinusoidally. **(E)** Generation of spin-3/2 rotations by driving three transitions, with the outer drives scaled by $\sqrt{3}/2$. The π-rotation is 2 times as long as a spin-1/2 rotation. The dashed line shows $\langle \hat{Z} \rangle$.

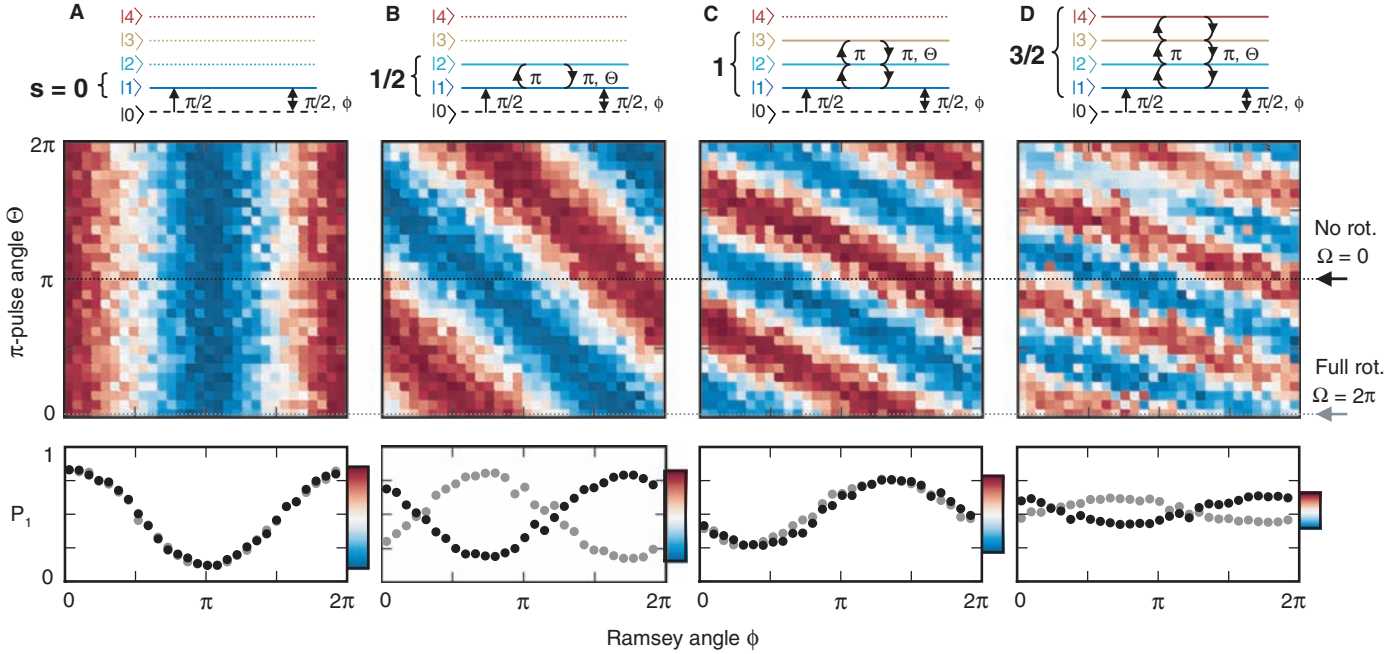

Fig. 4. Measurement of spin parity. The top panels show the microwave control sequence: The central π-pulses implement a closed-path spin rotation, whereas the outer π/2-pulses use Ramsey interference so as to detect the phase shift of $|1\rangle$. For spin-0, no π-rotations are applied. The middle panels show P_1 in color as a function of the angle Θ between the π-pulse rotation axes and the angle ϕ between the π/2-pulse rotation axes. The bottom panels show Ramsey fringe slices at Θ = π (Ω = 0 or no rotation; black) and Θ = 0 (Ω = 2π or one full rotation; gray), giving the relative phase shift due to a 2π-rotation. In-phase fringes (integer spins **A** and **C**) indicate a relative phase factor of 1, whereas out-of-phase fringes (half-integer spins **B** and **D**) indicate a relative phase factor of −1.

phase acquired by each spin under closed-path rotation, in particular the even parity of integer spins (and odd parity of half-integer spins) under 2π-rotation. This demonstration opens possibilities for using phase qudits in quantum information processing.

References and Notes

1. M. A. Nielsen, I. L. Chuang, *Quantum Computation and Quantum Information* (Cambridge Univ. Press, Cambridge, 2000).
2. A. Muthukrishnan, C. R. Stroud, *Phys. Rev. A* **62**, 052309 (2000).
3. B. Lanyon *et al.*, *Nat. Physics* **5**, 134 (2009).
4. I. Bregman, D. Aharonov, M. Ben-Or, H. S. Eisenberg, *Phys. Rev. A* **77**, 050301 (2008).
5. D. P. DiVincenzo, *Fortschr. Phys.* **48**, 771 (2000).
6. D. P. O'Leary, G. K. Brennen, S. S. Bullock, *Phys. Rev. A* **74**, 032334 (2006).
7. J. Clarke, F. K. Wilhelm, *Nature* **453**, 1031 (2008).
8. M. Steffen *et al.*, *Phys. Rev. Lett.* **97**, 050502 (2006).
9. M. Steffen *et al.*, *Science* **313**, 1423 (2006).
10. J. J. Sakurai, *Modern Quantum Mechanics* (Addison-Wesley, Reading, MA, 1994).
11. M. V. Berry, *Proc. R. Soc. Lond. A Math. Phys. Sci.* **392**, 45 (1984).
12. We worked in a rotating frame and chose the axis of rotation to be always perpendicular to the instantaneous spin direction $\langle \hat{\mathbf{S}} \rangle$, so that the dynamical phase is zero (*13*).
13. Materials and methods are available as supporting material on *Science* Online.
14. W. Pauli, *Phys. Rev.* **58**, 716 (1940).
15. I. Duck, E. C. G. Sudarshan, *Am. J. Phys.* **66**, 284 (1998).
16. H. Rauch *et al.*, *Phys. Lett.* **54A**, 425 (1975).
17. S. A. Werner, R. Colella, A. W. Overhauser, C. F. Eagen, *Phys. Rev. Lett.* **35**, 1053 (1975).
18. R. Kaiser, *Can. J. Phys.* **56**, 1321 (1978).
19. A. O. Niskanen *et al.*, *Science* **316**, 723 (2007).
20. A. Fragner *et al.*, *Science* **322**, 1357 (2008).
21. Because the global phase of a quantum system is undetectable, qudit states $|1\rangle$ and higher are used to emulate the spin, whereas the ground state $|0\rangle$ is reserved as phase reference. Hence, we emulated only up to spin-3/2, even though the 5-level qudit would map to an isolated spin-2.
22. M. Steffen, J. M. Martinis, I. L. Chuang, *Phys. Rev. B* **68**, 224518 (2003).
23. E. Lucero *et al.*, *Phys. Rev. Lett.* **100**, 247001 (2008).
24. M. Neeley *et al.*, *Phys. Rev. B* **77**, 180508 (2008).
25. G. K. Brennen, D. P. O'Leary, S. S. Bullock, *Phys. Rev. A* **71**, 052318 (2005).
26. H. Wang *et al.*, *Phys. Rev. Lett.* **101**, 240401 (2008).
27. M. Brune *et al.*, *Phys. Rev. Lett.* **101**, 240402 (2008).
28. J. M. Martinis *et al.*, *Phys. Rev. Lett.* **95**, 210503 (2005).

29. Devices were made at the UCSB Nanofabrication Facility, a part of the NSF-funded National Nanotechnology Infrastructure Network. This work was supported by the Intelligence Advanced Research Projects Activity (grant W911NF-04-1-0204) and NSF (grant CCF-0507227).

Supporting Online Material

www.sciencemag.org/cgi/content/full/325/5941/722/DC1
Materials and Methods
SOM Text
Figs. S1 and S2
References

12 March 2009; accepted 8 June 2009
10.1126/science.1173440

Folding DNA into Twisted and Curved Nanoscale Shapes

Hendrik Dietz,[1,2]* Shawn M. Douglas,[1,2,3] William M. Shih[1,2,3]†

We demonstrate the ability to engineer complex shapes that twist and curve at the nanoscale from DNA. Through programmable self-assembly, strands of DNA are directed to form a custom-shaped bundle of tightly cross-linked double helices, arrayed in parallel to their helical axes. Targeted insertions and deletions of base pairs cause the DNA bundles to develop twist of either handedness or to curve. The degree of curvature could be quantitatively controlled, and a radius of curvature as tight as 6 nanometers was achieved. We also combined multiple curved elements to build several different types of intricate nanostructures, such as a wireframe beach ball or square-toothed gears.

The sequences of DNA molecules can be engineered so that complex higher-order structures form as multiple double-helical segments connected through numerous turn regions. Programmable self-assembly based on DNA directed to branch in this way offers an attractive route to creating particular shapes on the 1- to 100-nm scale (*1*–*4*), as evidenced by its use in constructing two-dimensional (2D) crystals (*5*), nanotubes (*6*–*11*), and 3D wireframe polyhedra (*12*–*17*). More recently, oligonucleotide–"staple-strand"–assisted folding of a multiple-kilobase "scaffold strand" has been introduced as a powerful method to direct the self-assembly of custom-shaped, megadalton-scale, planar arrays of antiparallel helices connected through turn regions (*18*). In this "scaffolded–DNA-origami" method, each staple strand base pairs along part of its length with a complementary segment of the scaffold strand and then abruptly switches to base pair with another complementary scaffold segment that may be quite distant in the scaffold primary sequence. A single staple strand may pair with several scaffold-strand segments, in accordance with this switching strategy. Association with hundreds of such staple strands constrains the scaffold strand to helical paths that raster back and forth into a target antiparallel-array arrangement.

We recently extended DNA origami to 3D nanoconstruction with a design strategy that can be conceptualized as stacking corrugated sheets of antiparallel helices (*19*). The resulting structures resemble bundles of double helices constrained to a honeycomb lattice (an example is shown in Fig. 1A; also see figs. S7 to S24 for detailed examples of how staple strands can be programmed to link the scaffold strand into an antiparallel array of honeycomb-pleated helices). The number, arrangement, and individual lengths of helices can be tuned to produce a variety of 3D shapes; we have developed a graphical software tool to aid in the design process (*20*). In this experiment, we expand the design space of accessible DNA-origami shapes to include a rich diversity of nanostructures with designed twist and curvature.

In our honeycomb-array framework, every double helix has up to three nearest neighbors (Fig. 1A) and is designed to connect to each by antiparallel strand crossovers, which are covalent phosphate linkages in the same form as that found in naturally occurring Holliday junctions. For explanatory purposes, here we assume that only staple strands, and not the scaffold strand, can cross over to form a Holliday junction between adjacent double helices (*19*). Every 7 base pairs (bp), the helical path of a strand rotates by 240°, assuming a B-form–DNA twist density of 10.5 bp per turn. Therefore, 14 bp gives rise to a rotation of 120° plus 360°, and 21 bp gives rise to a rotation of 0° plus two times 360°. As a result, antiparallel strand crossovers to one of the three nearest neighbors at 0°, 120°, and 240° can be engineered to occur once every 7 bp. Thus, along the helical axis of the whole honeycomb array, crossovers only can occur at positions that coincide with conceptual planes perpendicular to that axis spaced at 7-bp intervals.

These crossover planes can be used as a reference to conceive the honeycomb-pleated helix bundle as a 3D array of cells that by default each contain a 7-bp-long double-helical DNA fragment (Fig. 1B) that is mechanically coupled to its nearest neighbors. This abstraction of the DNA bundle as a collection of array cells is key for understanding how site-directed insertions and deletions of base pairs in the bundle can control twist and curvature.

We systematically adjusted the number of base pairs in selected subsets of array cells to realize DNA shapes that globally twist or bend along their helix-parallel axes. Because any array-cell DNA fragment is physically constrained by its neighbors in the honeycomb array, deletion of a base pair results in a local overwinding and tensile strain for that fragment, which causes it to exert a left-handed torque and a pull on its neighbors (Fig. 1C, top). The overwind strain can be relieved by a compensatory global left-handed twist of the bundle along its

[1]Department of Cancer Biology, Dana-Farber Cancer Institute, Boston, MA 02115, USA. [2]Department of Biological Chemistry and Molecular Pharmacology, Harvard Medical School, Boston, MA 02115, USA. [3]Wyss Institute for Biologically Inspired Engineering, Harvard University, Cambridge, MA 02138, USA.

*Present address: Physik Department and CiPSM, Technische Universität München, D-85748 Garching bei München, Germany. †To whom correspondence should be addressed. E-mail: william_shih@dfci.harvard.edu

ERRATUM

Post date 23 October 2009

Reports: "Emulation of a quantum spin with a superconducting phase qudit" by M. Neeley *et al.* (7 August, p. 722). Reference 20 cited the wrong paper. The correct reference 20 is "P. J. Leek *et al.*, *Science* **318**, 1889 (2007)."